International Journal of Vehicle Design

ISSN online: 1741-5314 - ISSN print: 0143-3369
https://www.inderscience.com/ijvd

Investigation of drivetrain dynamics on low-μ ground using the brush model

Jianing Yang, Georg Jacobs, Achim Kramer

DOI: 10.1504/IJVD.2024.10061815

Article History:

Received:	27 February 2018
Last revised:	25 June 2020
Accepted:	15 September 2021
Published online:	23 January 2024

Investigation of drivetrain dynamics on low-μ ground using the brush model

Jianing Yang*, Georg Jacobs and Achim Kramer

Institute for Machine Elements and Systems Engineering,
RWTH Aachen University,
Schinkelstrasse 10, 52062, Aachen, Germany
Email: YangJianing1988@gmail.com
Email: georg.jacobs@imse.rwth-aachen.de
Email: achim.kramer@imse.rwth-aachen.de
*Corresponding author

Abstract: This paper aims to investigate the influence of the low-friction ground on off-highway drivetrain dynamics. A comprehensive vehicle simulation model is established for this purpose. This vehicle model consists of three parts: the torsional drivetrain model, the vehicle body model of longitudinal dynamics and the tyre model with slip behaviour. To correctly reflect tyre slip behaviour, the brush model, which features a physical description of the tyre–ground contact patch, is applied. A group of simulations is carried out on the complete vehicle model, mainly from two perspectives: drivetrain eigen-modes and drivetrain transient response. For the drivetrain eigen-mode analysis, different tyre slip states and the transition process between these two states are taken into consideration. For the drivetrain transient response, the vehicle is assumed to drive over a patch of low-μ ground. The drivetrain oscillation is analysed, and factors such as driving speed and low-μ ground length are investigated.

Keywords: low-μ ground; tyre slip model; brush model; torsional drivetrain model; drivetrain eigen-modes; drivetrain transient response.

Reference to this paper should be made as follows: Yang, J., Jacobs, G. and Kramer, A. (2024) 'Investigation of drivetrain dynamics on low-μ ground using the brush model', *Int. J. Vehicle Design*, Vol. 94, Nos. 1/2, pp.123–149.

Biographical notes: Jianing Yang started as a Research Engineer in the field "Off-Highway" at Institute for Machine Elements and Systems Engineering since 2014. He mainly works on the analysis of multi-body model for mobile machines, by considering the interactions between drive train dynamics, driving behaviour and impact on ride comfort. In 2020, he received his doctor degree from RWTH Aachen University.

Georg Jacobs is a Director of the Institute for Machine Elements and Machine Design (IME) at the RWTH Aachen University since 2008. Since 2013 he is Director of the Chair for Wind Power Drives (CWD) and speaker of the board of the Center for Wind Power Drives (CWD) at the RWTH Aachen University. In the begging of 2018 the Institute for Machine Elements and Machine Design (IME) and the Institute for Chair and Institute for Engineering Design (ikt) were merged into the Institute for Machine Elements and System Engineering (MSE), and he has taken over as head of the institute.

Since 2013 Achim Kramer worked as a research engineer at the Institute for Machine Elements and Systems Engineering in the field of Off-Highway Drive Train Technology, where he became head of the research group system design in September 2014. In 2019, he received his doctor degree from RWTH Aachen University.

1 Introduction

Off-highway vehicles need to move over ground that offers less than ideal driving conditions, and unwanted dynamic oscillations can be caused and transferred to the drivetrain. These dynamic oscillations can affect driving comfort, lower the drivetrain efficiency and decrease the reliability of drivetrain components. Investigating these drivetrain mechanical vibrations is an important area of research in vehicle engineering. Typical investigated topics include shuffle (Bartram, 2011; Farshidianfar et al., 2000), rattle (Wang et al., 2001), judder (Centea et al., 1999) and clonk/clunk (Biermann and Hagerodt, 1999; Wehrwein and Mourelatos, 2009), which range from low-frequency drivetrain vibration (shuffle: 2–8 Hz drivetrain oscillation) to high-frequency noise (clonk/clunk: noise due to the backlash of a gear pair) (Bartram, 2011). The excitation sources for these vibrations are typically the operation of the power source (engine or motor) or the motion of drivetrain components (gear pair, clutches and shaft), which are all inside the vehicle. However, when off-highway vehicles drive over rough ground, the external excitation from the ground becomes also important for the drivetrain dynamics.

An ideal tyre–ground interaction guarantees that the traction power from the engine can be effectively delivered to move the vehicle forward. When the vehicle drives on slippery ground with a low friction coefficient, however, the tyre may not always generate sufficient traction force and may slide on the ground surface. Consequently, driving on low-μ ground can affect drivetrain eigen-frequencies (Bartram et al., 2010; Bartram, 2011; Pawar et al., 2007). Pawar et al. (2007) carried out a test of vehicle pull-away manoeuvres on a low-μ surface, i.e., icy ground, and found the driveshaft oscillating at 5.5 Hz. This frequency response could not be observed during a test of the vehicle driving on a high-μ surface. Bartram (2010, 2011) replicated the observed frequency on low-μ ground through modal analysis. He adopted two states (shown in Figure 1), sticking state and full-sliding state, as tyre boundary conditions to carry out the modal analysis of the drivetrain. The sticking state denotes that the tyre contact point adheres tightly to the ground, whereas the full-sliding state denotes that the contact point can slide over the ground. When the vehicle is on low-μ ground, the tyre can easily transit from the sticking state to the full-sliding state, which causes the migration of drivetrain eigen-frequencies (Bartram, 2011). Beyond the above studies, however, no other research has been reported that includes an in-depth investigation of the impact of low-μ ground conditions on drivetrain dynamics.

Figure 1 Two boundary conditions of tyre for drivetrain modal analysis (see online version for colours)

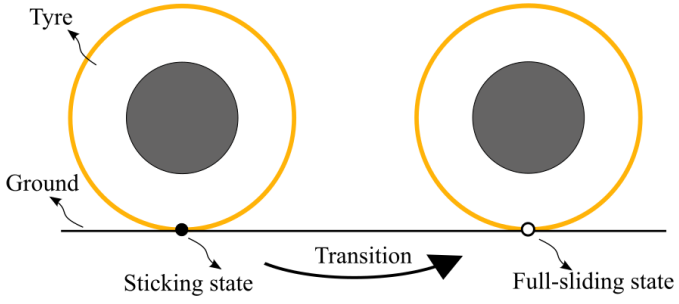

The present work aims to further investigate the influence of low-μ ground conditions on drivetrain dynamics through simulation techniques, with the focus mainly on the following two factors. First, the transition process from tyre sticking state to full-sliding state is taken into consideration for the drivetrain eigen-mode analysis. Second, the drivetrain transient response of a vehicle driving over a patch of low-μ ground is obtained and analysed. It is clear that the tyre slip behaviour is the key element for the analysis in this study. To account for these two factors, the tyre slip model must have the following two features:

1 a physical description of tyre contact area

2 a well-defined slip force curve (traction force vs. slip ratio) of the tyre.

Over recent decades, various tyre slip models haven been developed (Li et al., 2014), and they can be generally categorised into two types: the empirical models and the analytical models. The empirical models adopt a mathematical representation of the measured data, and the primary representative of them is the Magic Formula (Pacejka and Bakker, 1992; Pacejka, 2005). The Magic Formula is able to effectively describe the relationship between the slip force and slip ratio, but it lacks a physical description of the tyre contact patch. The analytical methods, by contrast, normally use a physical description for the tyre contact patch, and the "brush concept" may be the approach most widely used in forming an analytical slip model. A brush model (Dugoff et al., 1969; Fancher and Bareket, 1992; Gim and Nikravesh, 1990) utilises a group of elastic bristles to represent the tread element. Consequently, the physical status (sliding or adhesion) of each bristle in the contact area can be determined. The brush model can be also used to describe the relationship between the slip ratio and the developed slip force. The classic form of the brush model can describe the slip force curve at small slip ratios well, but its deficiency is that it is not able to predict the decaying characteristic of this curve at larger slip ratios (Zegelaar, 1998). To compensate for this drawback, Svendenius (2007) utilises velocity-dependent friction to replace the constant friction coefficient. The resulting developed slip force curve is able to reflect the decrease of the slip force at large slip ratios. Another advantage of the brush model is that it is able to explain the transient effect of the tyre slip model. Under realistic conditions, the tyre slip force does not develop immediately after a manoeuvre but requires a certain rolling distance for the force to build up (Svendenius, 2007). A practical method is to adopt a so-called relaxation length to

describe this dynamic behaviour (Clover and Bernard, 1998), and the brush model can be used to derive this relaxation length.

Besides the tyre slip model, a suitable drivetrain model is also needed in this study. The most common method to investigate drivetrain oscillation is to establish a torsional drivetrain model. In a typical torsional model, all components of the drivetrain are simplified into rotating inertia, spring and damper. Under such conditions, the mass of the vehicle body is also represented by equivalent inertia. This kind of model is widely used for investigating different drivetrain torsional vibration phenomena (Centea et al., 1999; Couderc et al., 1998; Oh and Singh, 2005; Wehrwein and Mourelatos, 2009). As a slight improvement of the torsional drivetrain model, a drivetrain model with longitudinal vehicle dynamics accounts for the longitudinal motion of the vehicle body as well (Mavros, 2010). Incorporating the longitudinal dynamics of the vehicle body makes its fore–aft motion visible, and this fore–aft motion is closely related to the lowest drivetrain eigen-mode.

In this study, an in-depth analysis is conducted to investigate the influence of low-μ ground condition on drivetrain dynamics. Consequently, a complete vehicle model is built, and the brush model is used to model the tyre slip behaviour. Using the simulation model, the drivetrain eigen-modes and the transient response of the vehicle driving on or over the low-μ ground are obtained. A novel approach made by this study is that: in the drivetrain eigen-mode analysis, the slip ratio s is adopted as a system state. Traditionally, only the displacement and/or the velocity of the components are used to denote system states in the drivetrain modal analysis. In this work, however, the tyre slip ratio is adopted as well. With this adoption, the transition process of the tyre slip status (from sticking state to full-sliding state) is able to be reflected.

The paper is organised in the following way. In Chapter 2, the definition of the physical brush model is introduced. The mathematical formulations of the tyre slip model in both steady form and dynamic form are then derived, and some characteristics of the brush model are explained. The complete vehicle model is constructed in Chapter 3. Chapter 4 introduces the supporting mathematical method for modelling the dynamic system, which adopts the tyre slip ratio as the system state. In Chapter 5, the eigen-mode analysis of the drivetrain with different tyre contact states is carried out; the transient response of the vehicle when driving over a patch of low-μ ground is also investigated. The paper's conclusions are presented in Chapter 6.

2 Physical brush model

In this section, a detailed description of the brush model is given. First, the structure of the brush model is introduced, and the physical status within the contact patch is explained. The mathematical formulation of the brush model is then given. Finally, tyre dynamic slip behaviour is determined using the brush model.

2.1 Description of the brush model

The main assumption underlying the brush model is that the tread element can be represented as a group of elastic bristles. As shown in Figure 2, within the contact patch, one end of the bristle connects to the tyre belt and the other end contacts the ground. Each bristle can deflect in the longitudinal direction independently, and the interacting force of

the bristle is proportional to its deflection. With the tyre rolling movement, the bristle enters the contact patch from the front edge, and leaves from the rear edge. As an individual bristle enters the contact patch, its deflection increases linearly with the travel distance. The maximum longitudinal deflection and corresponding interacting force of each bristle are constrained by the pressure distribution and tyre–ground friction coefficient. Before reaching its maximum deflection, the bristle adheres to the ground (adhesion region); after the maximum deflection, the bristle slides on the ground (sliding region).

Figure 2 Visualisation of the structure of the brush model (see online version for colours)

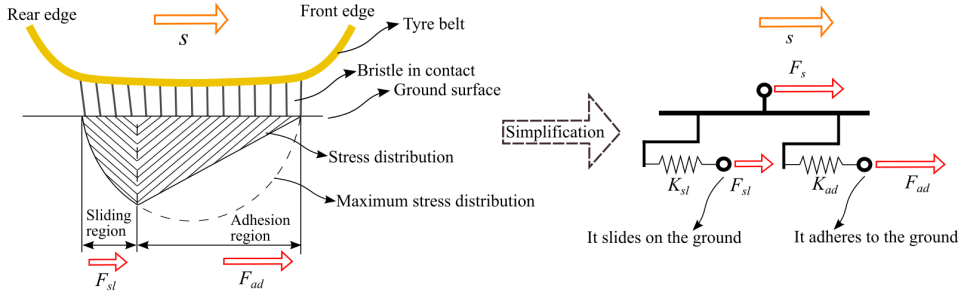

The right side of Figure 2 is the simplified description of the brush model. F_{sl} and F_{ad} represent the sliding force and adhesive force, and F_s ($F_s = F_{sl} + F_{ad}$) is the overall slip force inside the contact patch. K_{sl} and K_{ad} are the tread stiffness in the sliding region and adhesion region, respectively.

Figure 3 shows the explanation of the slip force composition based on the brush model. In the left part of Figure 3, the original sliding region and adhesion region at slip ratio s are depicted. With a small variation of the slip ratio Δs, adhesion region and sliding region change their lengths and the updated slip force $F_s^{'}$ becomes

$$F_s^{'} = F_s + \Delta F_s \tag{1}$$

where F_s is the original slip force and ΔF_s is the variation of the slip force. In the right part of Figure 3, the composition of the adhesive force and sliding force are depicted. The updated adhesive force $F_{ad}^{'}$ can be expressed as

$$F_{ad}^{'} = F_{ad1} + \Delta F_{ad} \tag{2}$$

F_{ad1} is part of the original adhesive force F_{ad} ($F_{ad} = F_{ad1} + F_{ad2}$), and ΔF_{ad} is the variation of the adhesive force. The sliding force $F_{sl}^{'}$ with the slip ratio variation can be calculated through

$$F_{sl}^{'} = F_{sl} + \Delta F_{sl} \tag{3}$$

where F_{sl} is the original sliding force and ΔF_{sl} is the sliding force variation.

Figure 3 The explanation of the slip force composition (see online version for colours)

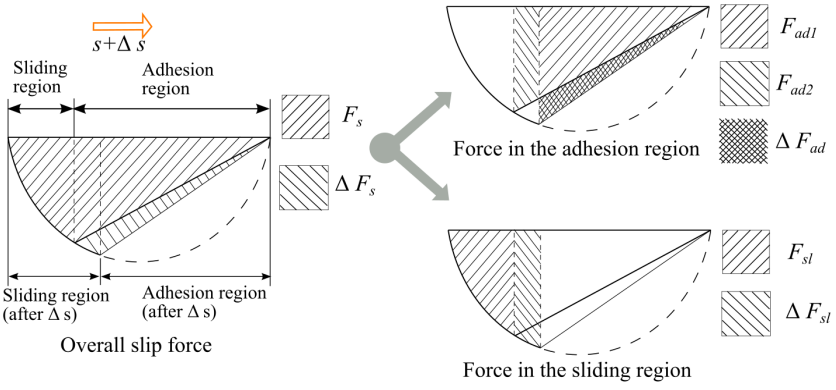

Therefore, the variation of the overall slip force ΔF_s is

$$\Delta F_s = \Delta F_{ad} + \Delta F_{sl} - F_{ad2} \tag{4}$$

The variation ΔF_s happens only in the original adhesion region, which indicates that the slip force variation ΔF_s would transfer to the tyre only through the tread elements in the adhesion region. Thus, the stiffness K_{ad} (Figure 2) is considered as the effective stiffness helping the tyre "stick" to the ground.

2.2 *Mathematical formulation of the tyre slip model in the steady form*

As shown in Figure 4, a parabolic form of the pressure distribution in the contact patch is assumed, which is expressed as

$$p(\xi) = 4p_m \frac{\xi}{l_c}(1 - \frac{\xi}{l_c}) \tag{5}$$

where p_m is the maximum value of the pressure distribution, l_c is the contact length and ξ denotes the location in the contact patch. The relation between the total normal load F_n and the maximum pressure p_m is calculated by integrating the pressure over the contact patch, which forms the relation $p_m = 3F_n / (2l_c)$.

Figure 4 Parabolic pressure distribution in the contact patch

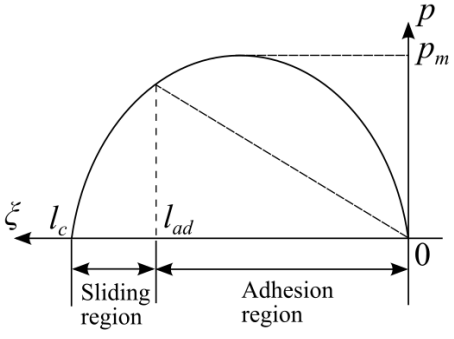

For pure longitudinal condition, the slip ratio s of the tyre is defined as

$$s=\begin{cases}\dfrac{v_x-r_e\omega}{v_x} & \textit{braking}\\ \dfrac{r_e\omega-v_x}{r_e\omega} & \textit{traction}\end{cases} \tag{6}$$

where v_x is the tyre longitudinal velocity, ω is the tyre angular velocity, and r_e is the tyre effective radius. During the traction process, the deflection of the bristle in the adhesion region is

$$\delta(\xi)=\frac{r\omega-v_x}{r\omega}\xi=s\xi \qquad 0\le\xi<l_{ad} \tag{7}$$

In equation (7), l_{ad} is the length of the adhesion region. The resulting interacting force in the adhesion region can be calculated by integrating bristle forces over the contact patch, that is

$$F_{ad}=\int_0^{l_{ad}}k_{tr}\delta(\xi)\,\mathrm{d}\xi=\frac{1}{2}k_{tr}{l_{ad}}^2 s \tag{8}$$

where k_{tr} is the average tread stiffness per unit length. In the sliding region, the sliding friction between the tyre and the ground is denoted as μ_x. Accordingly, the integrated force in the sliding region is

$$F_{sl}=\int_{l_{ad}}^{l_c}\mu_x p(\xi)\,\mathrm{d}\xi=4\mu_x p_m\left[\frac{1}{2}\frac{{l_c}^2-{l_{ad}}^2}{l_c}-\frac{1}{3}\frac{{l_c}^3-{l_{ad}}^3}{{l_c}^2}\right] \tag{9}$$

At the point $\xi=l_{ad}$, the relation $\mu_x p(\xi)=k_{tr}\delta(\xi)$ exists. Thus, the value of l_{ad} can be expressed as

$$l_{ad}=\frac{4\mu_x p_m-k_{tr}l_c s}{4\mu_x p_m}l_c \tag{10}$$

By Combining equations (8)–(10) and the relation $p_m=3F_n/(2l_c)$, the overall traction force can be obtained, which is as follows

$$F_s=F_{ad}+F_{sl}=\begin{cases}\mu_x F_n\left[3\dfrac{s}{\Lambda}-3\left(\dfrac{s}{\Lambda}\right)^2+\left(\dfrac{s}{\Lambda}\right)^3\right] & 0\le s<\Lambda\\ \mu_x F_n & s\ge\Lambda\end{cases} \tag{11}$$

with $\Lambda=4\mu_x p_m/(k_{tr}l_c)$.

In order to reflect the decrease of the traction force at large slip ratio, the velocity-dependent friction coefficient is adopted (Svendenius, 2007). Therefore, a nonlinear velocity-dependent friction parameter g_v is introduced. g_v is a function describing the Stribeck effect of dry friction (Wojewoda et al., 2008), which can be expressed as (Svendenius, 2007)

$$g_v = \mu_k + (\mu_s - \mu_k)e^{-(|v_r|/v_s)^\gamma} \tag{12}$$

where μ_k and μ_s are the kinetic and static Coulomb friction coefficients, v_r is the relative velocity between contacting parts, v_s is the Stribeck characteristic velocity, and γ is the shape factor of the Stribeck curve. In the following, $\mu_{sl}g_v$ is utilised to replace μ_x in equation (11) and the value of μ_{sl} can represent different ground conditions: in this study, μ_{sl} is set to be 0.8, 0.5, 0.2, and 0.1 to represent dry asphalt, wet asphalt, snow and ice, respectively (Deur et al., 2004). Then the slip force curve can be expressed with the following equation.

$$F_s = \begin{cases} \mu_{sl}g_v F_n \left[3\dfrac{s}{\Lambda} - 3\left(\dfrac{s}{\Lambda}\right)^2 + \left(\dfrac{s}{\Lambda}\right)^3 \right] & 0 \le s < \Lambda \\ \mu_{sl}g_v F_n & s \ge \Lambda \end{cases} \tag{13}$$

with $\Lambda = 4\mu_{sl}g_v p_m / (k_{tr} l_c)$.

Figure 5 shows the comparison between the predicted curve of the brush model and the measured data of two tractor tyres (Witzel, 2016). It can be seen that the brush model with velocity-dependent friction could well describe the actual slip force at both small and large slip ratios. Figure 6 shows the traction force predicted by the brush model on different ground conditions. The adopted parameter values of the brush model for Figures 5 and 6 are shown in Table 1.

Figure 5 Comparison between the predicted curve of the brush model and measured curves from the literature (see online version for colours)

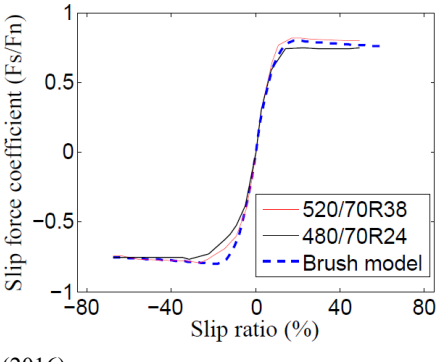

Source: Witzel (2016)

Figure 6 Tyre slip behaviour with different levels of ground friction (see online version for colours)

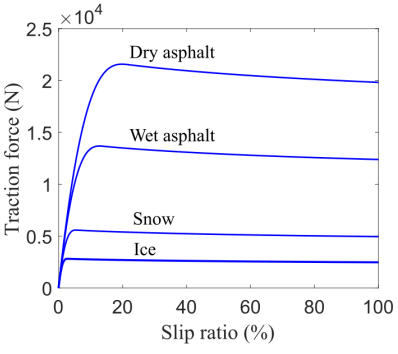

Table 1 Parameter values adopted for the brush model in Figures 5 and 6

Name	*Value*
μ_k	0.83
μ_s	1.06
v_s	4.2 m/s
γ	0.72
v_r	4 m/s
l	0.405 m
k_{tr}	3.6×10^6 N/m^2
$\boldsymbol{F_n}$	27000 N

2.3 Dynamic form of the tyre slip model

The diagram in Figure 7 is used to explain the dynamic effect based on the brush model, which incorporate the concept of relaxation length (Clover and Bernard, 1998). As shown in Figure 7, the tyre is rolling with the angular velocity ω, and the forward velocity is v_x. Point A_1 and point A_2 are assumed to be attached to the centre of the belt and contact patch, and their longitudinal velocities, v_s and v_{sc}, are used to denote the velocities of the belt and the contact patch, respectively. Thus, the belt velocity is

$$v_s = r_e\omega - v_x \tag{14}$$

where r_e is tyre radius (not displayed in Figure 7). Point A_1 and point A_2 are considered to be connected through a spring, whose stiffness results from the deformation of bristles. The variation of the force between point A_1 and point A_2 can be calculated as

$$\Delta F_s = K_{ad}\Delta x \tag{15}$$

where K_{ad} is the effective stiffness and x is the longitudinal distance between point A_1 and point A_2. As shown in Figure 8, the slip stiffness is defined as the ratio of the slip force to the slip ratio, which is

$$C_s = \frac{\Delta F_s}{\Delta s} \tag{16}$$

Inserting equation (15) into equation (16), the following relation is obtained

$$C_s = K_{ad} \frac{\Delta x}{\Delta s} \tag{17}$$

Substituting the relation $\Delta x / \Delta t = v_s - v_{sc}$ into equation (17) yields

$$\frac{\Delta s}{\Delta t} C_s = K_{ad} (v_s - v_{sc}) \tag{18}$$

The transient slip ratio s is defined as

$$s = \frac{v_{sc}}{r_e \omega} \tag{19}$$

Please note that when the tyre is rolling at a steady state, the relation $v_s = v_{sc}$ exists. Then the slip ratio defined in equation (19) is the same as the traction slip ratio shown in equation (6).

Figure 7 Explanation of the dynamic effect based on the brush model (see online version for colours)

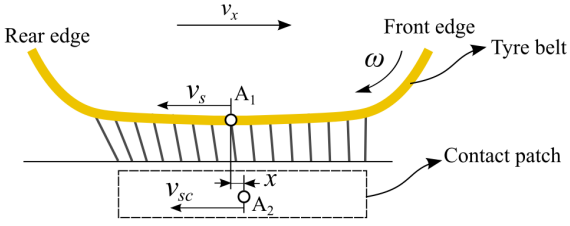

Figure 8 Slip stiffness is defined as the ratio of the slip force to the slip ratio (see online version for colours)

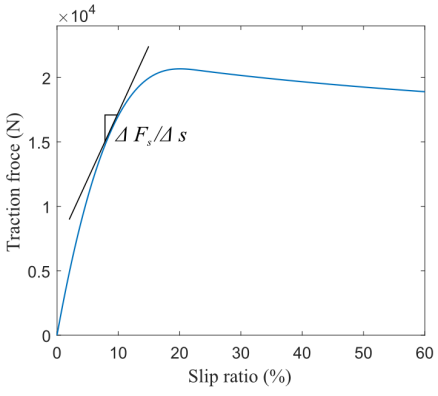

Substituting equation (19) into equation (18), the first-order equation of the slip ratio is obtained

$$C_s\dot{s} + K_{ad} r_e \omega s = K_{ad} v_s \tag{20}$$

Equation (20) can be transformed into the following form

$$\sigma_s \dot{s} + r_e \omega s = v_s \tag{21}$$

with the relaxation length $\sigma_s = C_s / K_{ad}$. Equation (21) describes the dynamic relation between the slip velocity v_s and the slip ratio s. After obtaining the value of the slip ratio s, the resulting slip force can be calculated through equation (13).

Figure 9(a) shows a velocity changing over time, which is used as the input to equation (21). Figure 9(b) shows the corresponding transient traction force response with different time scale t_0. Due to the introduction of the dynamic model in equation (21), the transient traction force shows a delay compared to the quasi-static response. With a short period t_0 (e.g., 0.1 s), the "delay" effect of the transient model becomes rather obvious, and simply adopting the quasi-static slip curve could lead to wrong traction force predictions. Hence, in order to investigate the correct influence of the dynamic slip behaviour on the drivetrain, the transient slip model should be considered.

Figure 9 The transient behaviour of the tyre slip (traction) force: (a) the input changing velocity for transient traction force response and (b) the transient traction force response with different time scales (see online version for colours)

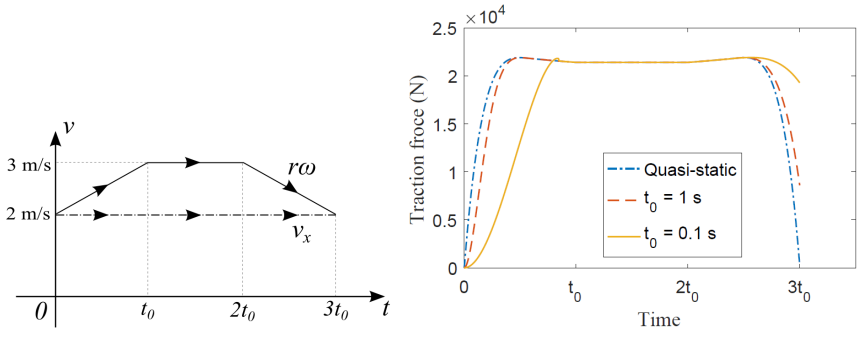

3 Introduction of the complete vehicle model

As shown in Figure 10, the complete vehicle model consists of three parts: the torsional drivetrain model, the vehicle body model and the tyre model. Figure 10(a) shows the torsional drivetrain model established in this study. This model is a half-vehicle model, which means the left side and right side of the vehicle are assumed to be symmetric. The model contains the engine, torque converter, two-stage gearbox with centre differential, shafts and axles. The output sides of the axles are connected to the torsional parts of the tyres. The scenario for each simulation in the following is that the vehicle drives at a constant speed. Consequently, the torque converter works at the locked status, and the gear ratio of the gearbox remains constant in each simulation. Figure 10(b) shows the vehicle body model with longitudinal dynamics. The vertical vehicle body motion is not included here, because the ground surface is assumed to be flat. Accordingly, the tyre

model, shown in Figure 10(c), does not include the vertical dynamics as well. The longitudinal and torsional springs and dampers represent the tyre sidewall compliance, and the rigid ring represents the tyre belt. The traction force is generated through the tyre slip behaviour, in which the brush model is used.

Figure 10 The complete vehicle model with vehicle longitudinal dynamics: (a) the torsional drivetrain model; (b) the vehicle body model (longitudinal dynamics) and (c) the adopted tyre model with traction (slip) force (see online version for colours)

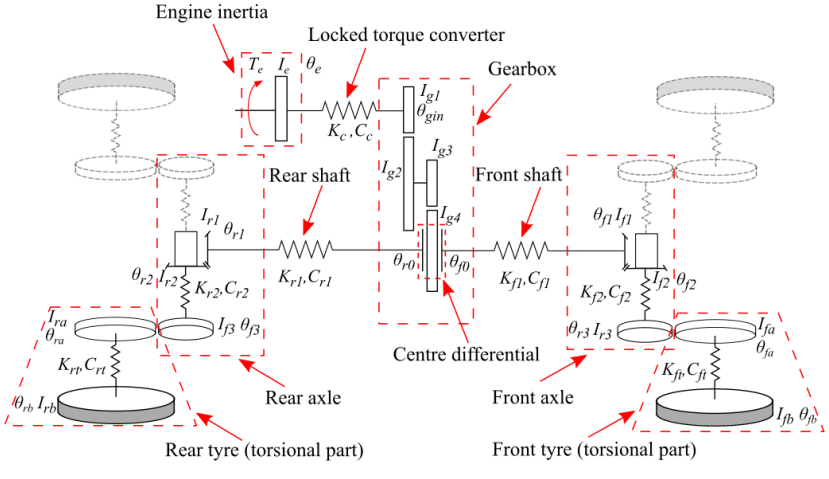

(a)

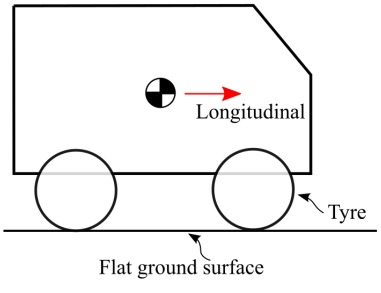

(b)

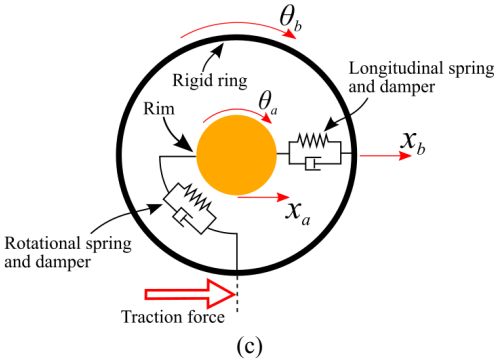

(c)

In Tables A1 and A2 (Appendix), the necessary parameters of the drivetrain model are listed. Table A1 shows the mass/inertia, stiffness and damping for the model. Table A2 shows ratios of the gear pair in the drivetrain model.

4 Supporting mathematical method for the complete vehicle model

In this section, the supporting mathematical method to model the complete vehicle (shown in Figure 10) is introduced. As shown in Figure 11, the tyre model is used as an example to explain the mathematical method. Afterward, the same method is used to obtain the eigen-modes of the complete vehicle model and the transient response of vehicle driving over low-μ ground.

Figure 11 Tyre model with traction (slip) force (see online version for colours)

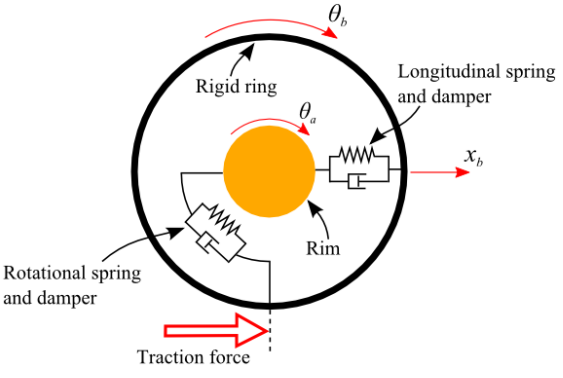

Figure 11 shows the structure of the tyre model. The rim rotates around its centre and the rotational angle is coupled with the drivetrain torsional movement. The rigid ring, which represents the tyre belt, is assumed to contact the ground. With the tyre slip behaviour, a traction force is produced to move the tyre forward. Accordingly, the drivetrain torsional movement is coupled with the vehicle longitudinal dynamics through this tyre model. For the convenience of the explanation, the rim is assumed to move with a constant velocity in the longitudinal direction, thus the rim's displacement x_a does not appear in the dynamic equations.

Mathematical equations for the tyre model shown in Figure 11 can be expressed as

$$I_a \ddot{\theta}_a + C_t\left(\dot{\theta}_a - \dot{\theta}_b\right) + K_t\left(\theta_a - \theta_b\right) = T_d \tag{22}$$

$$I_b \ddot{\theta}_b - C_t\left(\dot{\theta}_a - \dot{\theta}_b\right) - K_t\left(\theta_a - \theta_b\right) = -r_e F_s \tag{23}$$

$$M_b \ddot{x}_b + C_b \dot{x}_b + K_b x_b = F_s \tag{24}$$

where I_a is the rim inertia, I_b is the ring inertia, m_b is the ring mass, K_t is the tyre torsional stiffness, K_b is the tyre longitudinal stiffness, C_t is the torsional damping, C_b is the longitudinal damping, r_e is the effective tyre radius, F_s is the tyre slip (traction) force and T_d is the driving torque acting on the rim.

By reorganising equations (22)–(24), the following form is

$$\boldsymbol{M}\ddot{\boldsymbol{u}}_1 + \boldsymbol{C}\dot{\boldsymbol{u}}_1 + \boldsymbol{K}\boldsymbol{u}_1 = \boldsymbol{F}_1 \tag{25}$$

with

$$\boldsymbol{M} = \begin{bmatrix} I_a & 0 & 0 \\ 0 & I_b & 0 \\ 0 & 0 & M_b \end{bmatrix} \quad \boldsymbol{C} = \begin{bmatrix} C_t & -C_t & 0 \\ -C_t & C_t & 0 \\ 0 & 0 & C_b \end{bmatrix} \quad \boldsymbol{K} = \begin{bmatrix} K_t & -K_t & 0 \\ -K_t & K_t & 0 \\ 0 & 0 & K_b \end{bmatrix}$$

$$\boldsymbol{u}_1 = (\theta_a \quad \theta_b \quad x_b)^T$$

$$\boldsymbol{F}_1 = (T_d \quad -rF_s \quad F_s)^T$$

The dynamic slip model based on the equation (21) can be written in the following form

$$\boldsymbol{P}\dot{\boldsymbol{u}}_2 + \boldsymbol{Q}\boldsymbol{u}_2 = \boldsymbol{F}_2 \tag{26}$$

with

$$\boldsymbol{P} = [\sigma_s] \quad \boldsymbol{Q} = [r\omega]$$

$$\boldsymbol{u}_2 = (s)^T$$

$$\boldsymbol{F}_2 = (r\dot{\theta}_b - \dot{x}_b)^T$$

Then, combining equations (25) and (26), the following first-order equation is obtained

$$\boldsymbol{A}\dot{\boldsymbol{q}} + \boldsymbol{B}\boldsymbol{q} = \boldsymbol{F} \tag{27}$$

with

$$\boldsymbol{A} = \begin{bmatrix} \boldsymbol{M} & 0 & 0 \\ 0 & \boldsymbol{P} & 0 \\ 0 & 0 & \boldsymbol{I} \end{bmatrix} \quad \boldsymbol{B} = \begin{bmatrix} \boldsymbol{C} & 0 & \boldsymbol{K} \\ 0 & \boldsymbol{Q} & 0 \\ -\boldsymbol{I} & 0 & 0 \end{bmatrix}$$

$$\boldsymbol{q} = (\dot{\boldsymbol{u}}_1^T \quad \boldsymbol{u}_2^T \quad \boldsymbol{u}_1^T)^T$$

$$\boldsymbol{F} = (\boldsymbol{F}_1^T \quad \boldsymbol{F}_2^T \quad 0^T)^T$$

Equation (27) can be used to obtain the tyre dynamic response. For the complete vehicle model shown in Figure 10, the dynamic equations can also be organised in a form similar to equation (27), and the simulation for obtaining the drivetrain transient response with external excitations can be conveniently conducted.

To investigate the eigen-frequencies and mode shapes of the drivetrain, the linearisation of the system needs to be carried out. Noticing that the traction force F_s is a function of slip ratio s, the linearised form of F_s is

$$\hat{F}_s = C_s \hat{s} \tag{28}$$

where $\hat{F}_s$ and $\hat{s}$ represent finite variations of F_s and s by adding the symbol " ˆ ". Then, the following equation can be obtained

$$\hat{\boldsymbol{F}}_1 = \boldsymbol{N}\hat{\boldsymbol{u}}_2 + \hat{\boldsymbol{T}}_1 \tag{29}$$

with

$$\boldsymbol{N} = \begin{bmatrix} 0 & -r_e C_s & C_s \end{bmatrix}^T$$

$$\hat{\boldsymbol{T}}_1 = (\hat{T}_d \quad 0 \quad 0)^T$$

$\hat{\boldsymbol{F}}_2$ can be represented by using $\hat{\boldsymbol{u}}_1$, which is shown as follows

$$\hat{\boldsymbol{F}}_2 = \boldsymbol{R}\dot{\hat{\boldsymbol{u}}}_1 \tag{30}$$

with

$$\boldsymbol{R} = [0 \quad r_e \quad -1]$$

Thus, the linearised version of equation (27) becomes

$$\boldsymbol{A}^*\dot{\hat{\boldsymbol{q}}} + \boldsymbol{B}^*\hat{\boldsymbol{q}} = \hat{\boldsymbol{T}} \tag{31}$$

with

$$\boldsymbol{A}^* = \begin{bmatrix} \boldsymbol{M} & 0 & 0 \\ 0 & \boldsymbol{P} & 0 \\ 0 & 0 & \boldsymbol{I} \end{bmatrix} \quad \boldsymbol{B}^* = \begin{bmatrix} \boldsymbol{C} & -\boldsymbol{N} & \boldsymbol{K} \\ -\boldsymbol{R} & \boldsymbol{Q} & 0 \\ -\boldsymbol{I} & 0 & 0 \end{bmatrix}$$

$$\hat{\boldsymbol{q}} = (\dot{\hat{\boldsymbol{u}}}_1^T \quad \hat{\boldsymbol{u}}_2^T \quad \hat{\boldsymbol{u}}_1^T)^T$$

$$\hat{\boldsymbol{T}} = (\hat{\boldsymbol{T}}_1 \quad 0^T \quad 0^T)^T$$

By solving the eigen-value problem of $\left|\boldsymbol{A}^*\lambda + \boldsymbol{B}^*\right| = 0$, corresponding eigen-frequencies and mode shapes can be obtained. For the complete drivetrain model, after organising the equations in the form of equation (31), eigen-modes of the drivetrain model under various tyre slip states can be analysed.

5 Dynamic simulation of the complete vehicle model

In this section, a group of analyses is conducted on an off-highway drivetrain under the condition of a vehicle driving on or crossing over low-μ ground. Investigations are mainly conducted through simulation methods, which aim to study the drivetrain characteristics from two perspectives: drivetrain eigen-modes and drivetrain transient response. Drivetrain eigen-modes, including the drivetrain's eigen-frequencies and mode shapes, are investigated by solving the eigen-value problem of the drivetrain. The tyre slip state is considered as the boundary condition to the drivetrain. In addition, due to the adoption of the brush model, not only the two contact states (sticking state and full-sliding state) but also the transition process between these two states can be used during the simulation. The transient simulation is conducted mainly to explore the drivetrain

dynamic response when the vehicle passes over a patch of low-μ ground. When the tyre stays on low-μ ground and cannot generate enough traction force, a sudden change of the traction force occurs, which further leads to an oscillation in the drivetrain. Through the simulation and the adopted tyre slip model, the mechanism causing drivetrain oscillation is explained. Furthermore, a group of influencing factors is investigated to study their effect on the severity of drivetrain oscillation.

5.1 Eigen-modes of the complete vehicle model

In this section, the eigen-modes of the complete vehicle model are obtained with the assistance of the previously introduced mathematical method. The goal is to investigate the influence of the tyre slip states on the drivetrain eigen-modes.

5.1.1 Eigen-modes of the drivetrain model under different boundary conditions

In the eigen-mode analysis of this subsection, the following assumption is made: when the tyre is on high-μ ground, the tyre sticks to the ground; when the tyre is on low-μ ground, the tyre slides over the ground. Therefore, the following three situations are considered:

1 front and rear tyres are on high-μ ground;

2 the front tyre is on low-μ ground while the rear tyre is on high-μ ground;

3 both front and rear tyres are on low-μ ground.

These three situations are shown in Figure 12(b)–(d), which are denoted as Case 1, Case 2 and Case 3, respectively. The gearbox is set to the second gear ratio (n_{g1}:1, n_{g2} : 2.84).

The calculated eigen-frequencies of different cases are shown in Table 2. From Table 2, it can be seen that the cases have differing values for their lowest eigen-frequency. In Case 1, the lowest eigen-frequency is 4.32 Hz. In Case 2, the front tyre slides along the ground, and the lowest eigen-frequency becomes 6.07 Hz. In Case 3, front and rear tyres both slide on the ground. Accordingly, the lowest eigen-frequency becomes 8.33 Hz.

Table 2 Calculated eigen-frequencies of the drivetrain under different tyre contact states

Frequency order	*1st* (Hz)	*2nd* (Hz)	*3rd* (Hz)	*4th* (Hz)	*5th* (Hz)	*6th* (Hz)
Case 1	4.32	10.62	13.39	26.78	26.95	27.59
Case 2	0	6.07	12.34	21.23	27.06	27.11
Case 3	0	0	8.33	20.83	21.61	26.99

The tyre contact status would affect not only the drivetrain eigen-frequency, but also the corresponding mode shape. In Figure 13, mode shapes under various boundary conditions are presented and the abbreviation for drivetrain positions is explained in Table 3.

Figure 12 Explanations of drivetrain simulation scenarios: (a) ground condition explanations; (b) case 1: front tyre and rear tyre are both on high-μ ground; (c) case 2: front tyre is on low-μ ground and rear tyre is on high-μ ground and (d) case 3: front tyre and rear tyre are both on low-μ ground (see online version for colours)

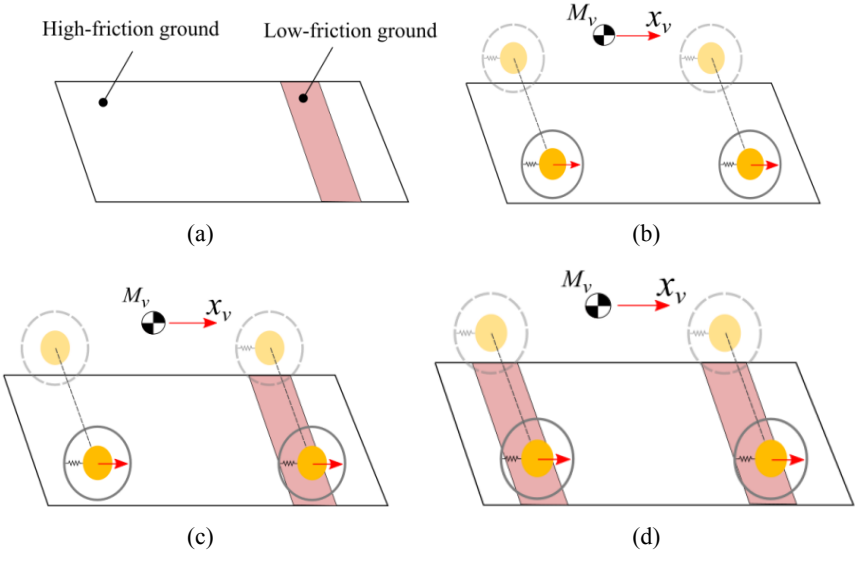

Figure 13 Mode shapes (corresponding to lowest eigen-frequency) of the drivetrain under different tyre contact states (see online version for colours)

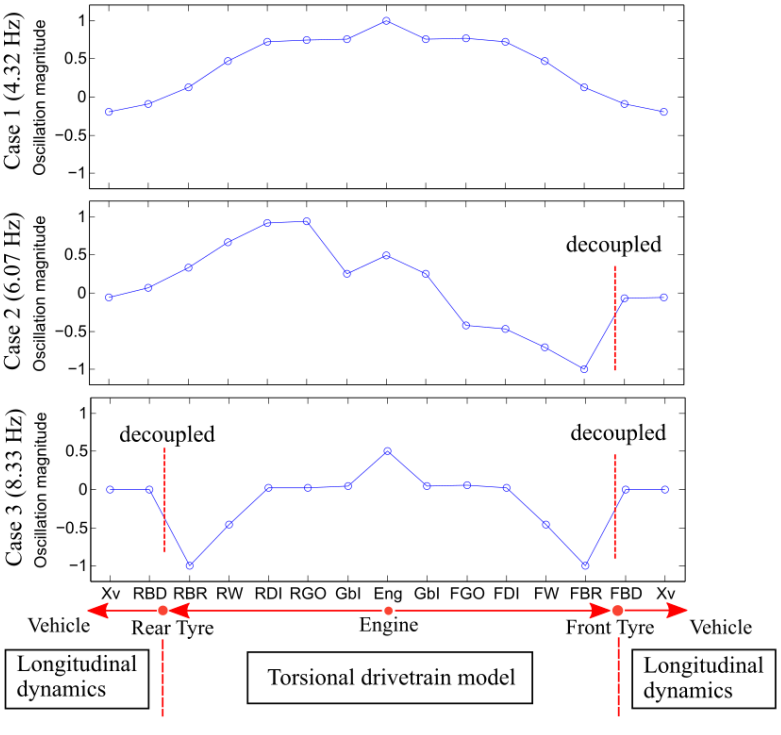

Table 3 The meaning of the abbreviation of the positions

Position	*Abbreviation*	*Position*	*Abbreviation*
Engine	Eng	Rear wheel	RW
Gearbox input	GBI	Front belt (torsional)	FBR
Gearbox front output	FGO	Rear belt (torsional)	RBR
Gearbox rear output	RGO	Front belt (longitudinal)	FBD
Front differential	FDI	Rear belt (longitudinal)	RBD
Rear differential	RDI	Vehicle	Xv
Front wheel	FW		

In Case 1, the mode shape shows characteristics similar to those seen in other literature (Bartram, 2011): the maximum motion magnitude occurs in the engine inertia, and the (longitudinal) vehicle body motion shows a negative direction. The oscillation magnitude of the tyre belt is very small when compared to the engine inertia.

In Case 2, motions of the FBR (torsional movement of the front belt) and FBD (longitudinal movement of the front belt) are decoupled. No constraint exists between the longitudinal and torsional movements of the front tyre, because this tyre has entered the full-sliding state. In addition, the oscillation magnitude of FBR is the largest.

In Case 3, the oscillation at the lowest eigen-frequency happens only inside the drivetrain, since both front tyre and rear tyres have entered the full-sliding states. Again, the maximum oscillation magnitude appears at the tyre belt (FBR and RBR).

5.1.2 Influence of the tyre transition process on the drivetrain eigen-frequency

As shown in Figure 1, the tyre could easily transit from the sticking state to full-sliding state on the low-μ ground. Accordingly, the eigen-frequency and mode shape of the drivetrain would change. In this subsection, the influence of the tyre transition process (from the sticking state to full-sliding state) on the drivetrain eigen-frequency is investigated.

According to the brush model, the tyre-to-ground sticking effect could be explained through the effective stiffness K_{ad}, which is the integrated tread stiffness in the adhesion region. When the tyre tries to produce more traction force on low-μ ground, the adhesion region becomes smaller. Consequently, the tyre-to-ground sticking effect becomes weaker. In order to describe the transition process, the so-called traction force ratio is given, which is defined as F_s / F_m. As shown in Figure 14, F_s is the generated traction force within the contact patch, whereas F_m is maximum traction force that the tyre can produce. The value of F_m is decided by the tyre normal load and the maximum friction coefficient between the tyre and ground. In the simulation in this subsection, the traction force ratio changes from 0% to 100% to reflect the tyre transition process: the 0% traction force ratio corresponds to the tyre sticking state, while the 100% traction force ratio denotes the full-sliding state.

Figure 14 The explanation of the traction force ratio (see online version for colours)

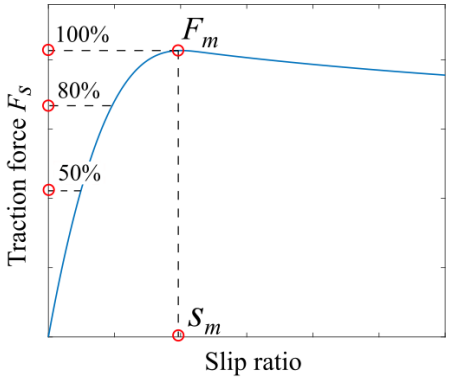

Figure 15 shows the simulation result of the influence of changing traction force ratio on the lowest eigen-frequency. Two conditions are considered:

1 only the front tyre traction force ratio changes

2 front and rear traction force ratios both change.

The changing eigen-frequencies of both curves show a similar trend: during most of the range of the traction force ratio (<90%), the frequency drops slightly; when the traction force ratio approaches 100% , the frequency drops quickly to 0 Hz. This indicates that the migration process of the eigen-frequency mainly happens inside a rather narrow range of the traction force ratio, and it might not be obvious in the frequency domain of the drivetrain dynamic simulation or test. In other words, when investigating the influence of tyre boundary condition on drivetrain eigen-frequency, two tyre slip states (sticking state and full-sliding state) should be enough for most analyses.

Figure 15 The variation of the lowest eigen-frequency during the transition from tyre sticking state to full-sliding state (see online version for colours)

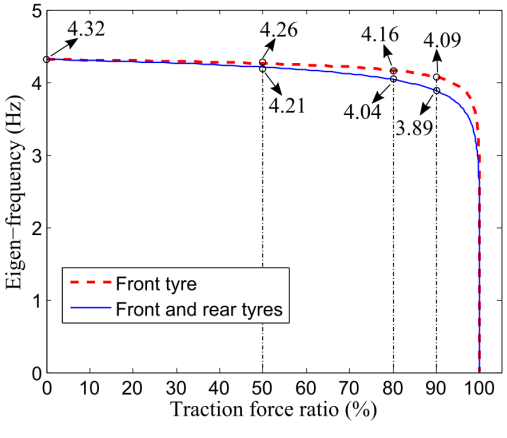

5.2 Transient response of the complete vehicle model

In this section, the vehicle is assumed to drive over a patch of low-μ ground, and its transient response is obtained. The gearbox output torque and the vehicle longitudinal acceleration are used as the main indicator to evaluate the oscillation/vibration severity.

5.2.1 The general explanation of the drivetrain dynamic response

The vehicle is assumed to drive over a patch of low-μ ground at a constant speed, as illustrated in Figure 16. When the vehicle moves forward, the front tyre meets low-μ ground first, followed by the rear tyre. In the simulation, the length of low-μ ground is set to be shorter than the vehicle's wheelbase. This means, at each moment, there will be at most one pair of tyres (either front tyres or rear tyres) on the low-μ ground. The resistance acting on the vehicle consists of three components: wind resistance, slope resistance and rolling resistance. The rolling resistance is added to the tyre as resistant torque. The wind and slope resistances are added to the vehicle body. The rolling resistance torque is calculated as $T_r = -r_e f_r F_n$, where f_r is the rolling resistance coefficient, r_e is the tyre effective radius, and F_n is the tyre normal load. The wind resistance is set to be zero. The slope resistance is calculated as $F_{resis} = -f_v F_v$, where f_v is the resistance coefficient, and F_v is the gravity force of the vehicle. Friction losses of the drivetrain are not considered in the simulation. During each simulation, a constant engine power is defined in order to propel the vehicle forward at a stable speed, and the set value of the engine power depends on the assumed driving speed and initial overall resistance.

The drivetrain dynamics in this simulation mainly refers to the torque/acceleration variation of the drivetrain/vehicle body. In the following, the torque of the output side of the gearbox (adding up of torques in the front and rear shafts) and the vehicle longitudinal acceleration are displayed.

The high-μ ground is dry asphalt ($\mu_{sl} = 0.8$). Three kinds of low-μ ground are adopted, which are wet asphalt ($\mu_{sl} = 0.5$), snow ($\mu_{sl} = 0.2$) and ice ($\mu_{sl} = 0.1$). In this simulation, the overall resistance (wind resistance, slope resistance and rolling resistance) is set to be between 10% and 20% of the complete vehicle weight ($f_r = 0.02$ and $f_v = 0.12$). This means the maximum produced traction force could be larger than the driving resistance when the vehicle stays on wet asphalt or snow; however, the maximum traction force is lower than the resistance on icy ground. The vehicle is assumed to drive at 12 km/h and the gearbox is at the second gear ratio. The vehicle wheelbase is 3m and the length of low-μ ground is 1.5 m. An open centre differential is considered to be installed at the gearbox output side, which means the torques occurring inside the front and rear shafts are same. The centre of gravity to the front tyre is assumed to be 1.5 m. Figure 17 shows the simulation results of the drivetrain oscillation when the vehicle drives over a patch of low-μ ground.

From Figure 17, the following phenomenon can be observed: when the vehicle drives over wet asphalt or snow, the oscillation is very small; however, when the vehicle drives over icy ground, the oscillation is rather severe. This phenomenon can be explained by Figure 18, which describes the variation of the tyre slip state.

Figure 16 The schematic diagram of the vehicle driving over a patch of low-μ ground (see online version for colours)

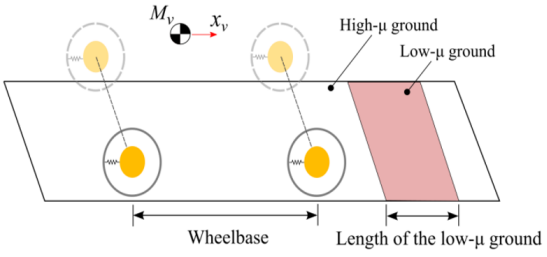

Overall vehicle mass (with tyre masses)	11000 kg
Driving speed	12 km/h,
Low-μ ground length	1.5 m
Wheelbase	3 m
Centre differential	Open
Gear ratio (gearbox)	2nd
Rolling resistance	$f_r = 0.02$
Initial slope resistance ratio	$f_v = 0.12$

Figure 17 Dynamic response of the vehicle driving over a patch of low-μ ground: (a) torque at the gearbox output side and (b) vehicle longitudinal acceleration (see online version for colours)

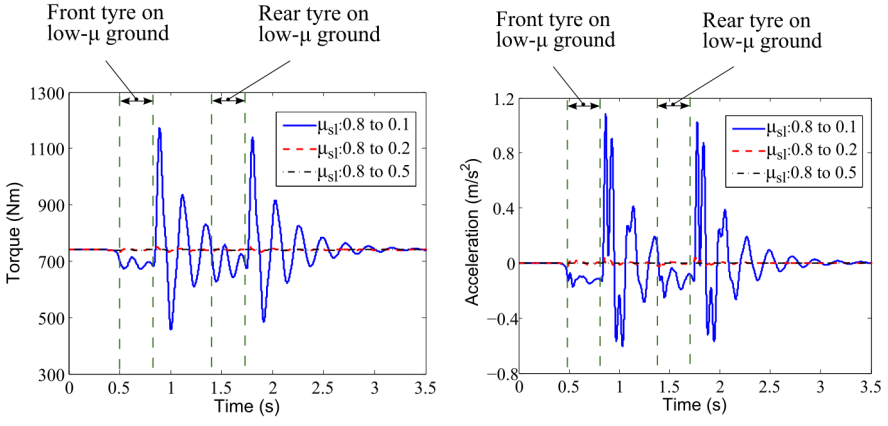

(a) (b)

Figure 18(a) could be used to explain conditions of the vehicle driving over wet asphalt ($\mu_{sl} = 0.5$) and snow ($\mu_{sl} = 0.2$). When the tyre enters the low-μ ground, the traction force would drop from point P_1 to point P_2. Afterward, in order to generate higher traction force, the point would move toward a higher slip ratio and become stabilised at point P_3. When the tyre re-enters the high-μ ground, the traction force jumps from point P_3 to point P_4 and finally returns to point P_1. The cycle $P_1P_2P_3P_4$ denotes the condition of the traction force variation for the tyre rolling over wet asphalt ($\mu_{sl} = 0.5$) and snow ($\mu_{sl} = 0.2$).

Figure 18(b) shows the situation when the vehicle drives over icy ground ($\mu_{sl} = 0.1$). When the tyre enters the low-μ ground, the traction force drops from point P_1 to point P_2. However, due to the limitation of the maximum friction coefficient, the tyre cannot generate enough traction force to reach the value of the needed force. Thus, unlike the condition in Figure 18(a), the traction force moves along the curve as long as the tyre stays on the low-μ ground. When the tyre returns to the high-μ ground, the traction force changes from point P_3 to point P_4, and then returns to point P_1. According to the condition described in Figure 18(b), the maximum variation occurs when the traction

force moves from point P_3 to point P_4, which is the time point when the tyre returns from low-μ ground to the high-μ ground.

Figure 18 The explanation of the tyre slip behaviour when this tyre rolls over low-μ ground ($F_{d,h}$ denotes the needed traction force to overcome resistance on the high-μ ground, while $F_{d,l}$ is the needed traction force on the low-μ ground. Normally, $F_{d,h} \geq F_{d,l}$): (a) stable process of the traction force variation and (b) unstable process of the traction force variation (see online version for colours)

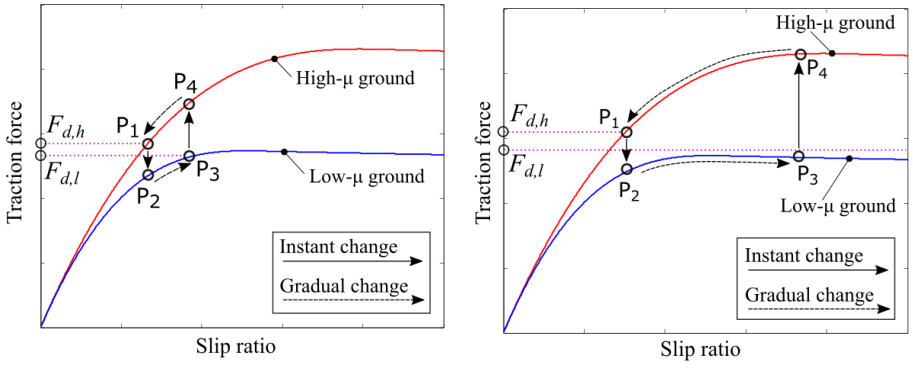

Comparing Figure 18(a) with Figure 18(b), the major difference between these two conditions is that in Figure 18(a), the traction force could reach a stabilised value; while in Figure 18(b), the traction force could never reach a stabilised value as long as the tyre stays on the low-μ ground. Therefore, the distance between point P_3 and point P_4 in Figure 18(b) would be much larger than that in Figure 18(a). Accordingly, the resulting oscillation of the drivetrain under the condition shown in Figure 18(b) would also be more severe than that in Figure 18(a).

5.2.2 Influence of low-μ ground length on drivetrain dynamic oscillation

As shown in Figure 19, on each torque oscillation curve, there appear two peak points and two valley points. These peak/valley points appear when the front or rear tyre returns to the high-μ ground. In the following, values of these points will be collected to indicate the severity of the drivetrain oscillation.

The vehicle is assumed to drive at a speed of 12 km/h, and crosses low-μ ground (μ_{sl} : 0.8–0.1) sections of different lengths ranging from 0.5 m to 2.5 m. These investigated lengths of low-μ ground are all shorter than the vehicle wheelbase (3 m), which guarantees that the torque oscillation of the gearbox follows the same pattern as shown in Figure 19.

Figure 20 shows the simulation result, which describes the values of the peak/valley points of the gearbox output torque. The deviation of peak/valley values from the unaffected value (740.2 Nm) denotes the drivetrain oscillation severity: a larger deviation denotes a more severe drivetrain oscillation. Two linear asymptotic lines are used to fit the variation of the peak values and valley values, respectively. The overall trend is that, with an increasing length of low-μ ground, the drivetrain oscillation becomes more severe. When the vehicle crosses 0.75 m of low-μ ground, the increase of the peak value

(based on the asymptotic line) reaches 27% compared to the unaffected torque value; as low-μ ground length is extended to 1.5 m and 2.25 m, the peak value increases by 59% and 91%, respectively, compared to the unaffected torque value. This phenomenon can be explained through Figure 18(b): when the tyre stays longer on the low-μ ground, the unstable process (point P_2 to point P_3) also becomes longer. Accordingly, the peak values, which are mainly influenced by the distance between point P_3 and point P_4, become higher. In addition, when the unstable process lasts longer, it takes a longer time to get back to the stable state (point P_1) after the tyre returns to high-μ ground. Therefore, when the section of low-μ ground is made longer, the oscillation magnitude increases.

Figure 19 The denotation of the peak/valley points on the oscillation curve (see online version for colours)

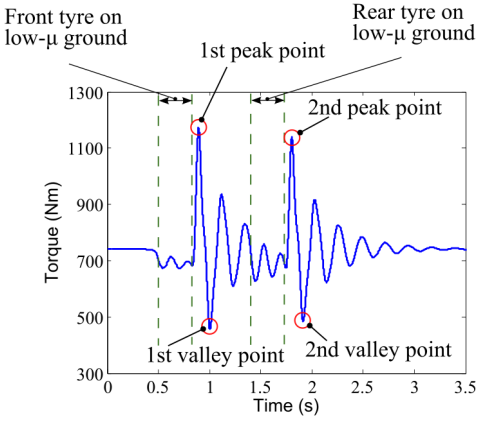

Figure 20 The variation of the peak/valley values of gearbox output torque at different low-μ ground lengths (driving at 12 km/h, μ_{sl} : 0.8 to 0.1) (see online version for colours)

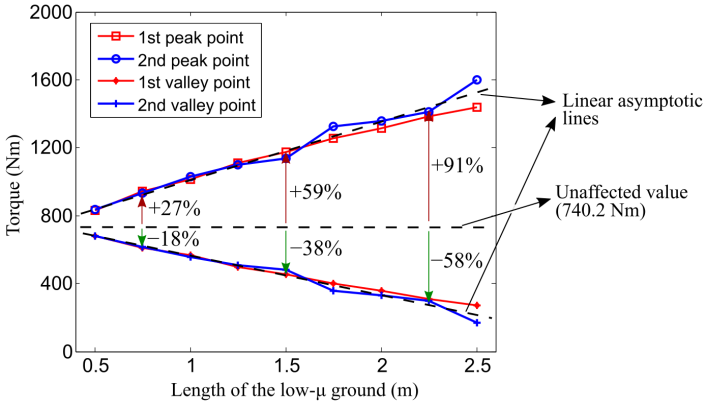

Another phenomenon can be found from Figure 20: values of the first peak/valley points are closer to a linear curve than those of the second peak/valley points. The reason is that the first peak/valley values appear just after the front tyre enters or leaves the low-μ ground, thus the values are influenced only by the slip state variation of the front tyre. However, when the rear tyre meets the low-μ ground, the drivetrain oscillation has not

yet been entirely damped (see Figure 19). Thus, the second peak/valley values are influenced not only by the slip state variation of the rear tyre but also by the previous drivetrain oscillation, which leads to some fluctuations of second peak/valley values. In general, when low-μ ground length is increased, the oscillation severity of the drivetrain would increase.

5.2.3 Influence of driving speed on drivetrain dynamic oscillation

This investigation evaluates the impact of driving speed on drivetrain oscillation. In this subsection, the length of low-μ ground is set to be 1.5 m, and the driving speed varies from 8 km/h to 15 km/h. This speed range was chosen based on the selected gear ratio (second gear ratio) and the engine output speed (800 rpm to 2400 rpm). The friction coefficient of the high-μ ground is 0.8, and that of low-μ ground is 0.1.

Figure 21 shows the gearbox torque variation when the vehicle drives over low-μ ground at various driving speeds. It can be seen that when the vehicle drives at a higher speed, the oscillation severity decreases. As denoted in Figure 21, when the vehicle drives at 9 km/h, the peak value (according to the asymptotic line) is 68% higher than the unaffected torque value. With higher driving speeds of 12 km/h and 15 km/h, the increases of high peak value become 59% and 51%, respectively. This trend can be explained, again, through Figure 18(b): when the speed is higher, the time the tyre spends on low-μ ground is shorter, which decreases the time period of the unstable process (point P_2 to point P_3). Similar to Figure 20, the trend of the variation of the first peak/valley values is rather smooth, while the variation of the second peak/valley values shows some fluctuations. A general conclusion is that when the vehicle drives over low-μ ground at higher driving speed, the oscillation severity of the drivetrain becomes smaller.

Figure 21 The variation of the peak/valley values of gearbox output torque at different driving speeds (1.5 m low-μ ground length, μ_{sl} :0.8 to 0.1) (see online version for colours)

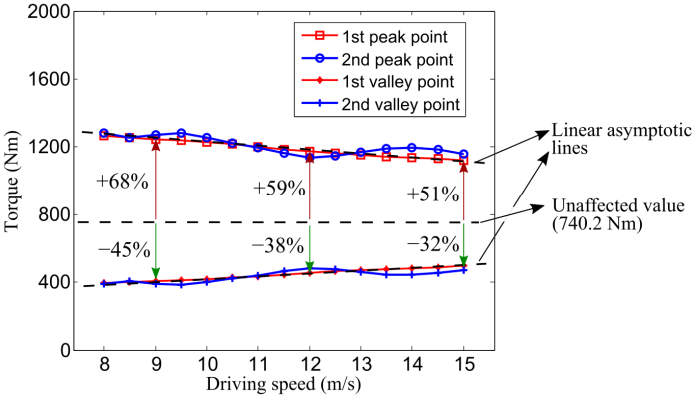

6 Conclusion

In this study, the influence of the low-μ ground on the drivetrain dynamics is investigated using a complete vehicle model. The complete vehicle consists of three parts: the torsional drivetrain model, the vehicle body model of longitudinal dynamics and the tyre

model with slip behaviour. The tyre slip behaviour is described using the brush model. Then, a group of simulations of the vehicle driving over low-μ ground are carried out. The main conclusions are as follows.

For the drivetrain eigen-mode investigation, the tyre slip state is an important influencing factor. When the tyre enters the full-sliding state on low-μ ground, it no longer sticks to the ground. As a consequence, the lowest eigen-frequency and corresponding mode shape change. In addition, the belt oscillation magnitude of this sliding tyre becomes significantly larger than the belt oscillation magnitude when the tyre sticks to the ground.

With the adoption of the brush model, the transition process from tyre sticking state to full-sliding state can be considered in the eigen-mode investigation. The traction force ratio (0% to 100%) is defined to indicate the tyre slip state: 0% for the fully sticking state and 100% for the full-sliding state. It is found that as the traction force ratio increases from 0% to 90%, the drivetrain eigen-frequency decreases only slightly. As the traction force continues to increase from 90% to 100%, however, the eigen-frequency changes significantly. This indicates that the migration process of the eigen-frequency happens within a narrow range of the traction force ratio (i.e., 90% to 100%). Therefore, for most drivetrain eigen-mode analyses, two tyre slip states (sticking and full-sliding) should be sufficient.

When the vehicle drives over low-μ ground, severe oscillations occur inside the drivetrain if the tyre cannot generate enough traction force to overcome the driving resistance. The maximum oscillation magnitude appears once the front or rear tyre re-enters high-μ ground from low-μ ground. It is also found that as long as front tyre or rear tyre stays longer on the low-μ ground, a more severe oscillation will result (for the four-wheel-drive vehicle with centre differential). In other words, the oscillation severity generally diminishes as the driving speed increases and as the length of low-μ ground travelled over becomes shorter.

References

Bartram, M. (2011) *Transient Tire Modelling for the Simulation of Drivetrain Dynamic Response under Low-to-Zero Speed Traction Manoeuvres*, PhD thesis, Loughborough University, Loughborough, UK.

Bartram, M., Mavros, G. and Biggs, S. (2010) 'A study on the effect of road friction on driveline vibrations', *Proceedings of the Institution of Mechanical Engineers, Part K: Journal of Multi-Body Dynamics*, Vol. 224, No. 4, pp.321–340.

Biermann, J.W. and Hagerodt, B. (1999) 'Investigation of the clonk phenomenon in vehicle transmissions–measurement, modelling and simulation', *Proceedings of the Institution of Mechanical Engineers, Part K: Journal of Multi-Body Dynamics*, Vol. 213, No. 1, pp.53–60.

Centea, D., Rahnejat, H. and Menday, M.T. (1999) 'The influence of the interface coefficient of friction upon the propensity to judder in automotive clutches', *Proceedings of the Institution of Mechanical Engineers, Part D: Journal of Automobile Engineering*, Vol. 213, No. 1, pp.245–258.

Clover, C.L. and Bernard, J.E. (1998) 'Longitudinal tire dynamics', *Vehicle System Dynamics*, Vol. 29, No. 4, pp.231–260.

Couderc, P., Callenaere, J., Der Hagopian, J., Ferraris, G., Kassai, A., Borjesson, Y., Verdillon, L. and Gaimard, S. (1998) 'Vehicle driveline dynamic behaviour: experimentation and simulation', *Journal of Sound and Vibration*, Vol. 218, No. 1, pp.133–157.

Deur, J., Asgari, J. and Hrovat, D. (2004) 'A 3D brush-type dynamic tire friction model', *Vehicle System Dynamics*, Vol. 42, No. 3, pp.133–173.

Dugoff, H., Fancher, P.S. and Segel, L. (1969) *Tire Performance Characteristics Affecting Vehicle Response to Steering and Braking Control Inputs*, Final Report, Highway Safety Research Institute, Institute of Science and Technology, The University of Michigan, Ann Arbor, MI, USA.

Fancher Jr., P.S. and Bareket, Z. (1992) 'Including roadway and tread factors in a semi-empirical model of truck tires', *Vehicle System Dynamics*, Vol. 21, Sup.001, pp.92–107.

Farshidianfar, A., Rahnejat, H., Ebrahimi, M. and Menday, M.T. (2000) 'Low frequency torsional vibration of vehicular driveline systems in shuffle', in Rahnejat, H., Ebrahimi, M., Whalley, R. (Eds.): *Multi-Body Dynamics: Monitoring and Simulation Techniques*, Professional Engineering Publishing Limited, London and Bury St Edmunds, pp.269–282.

Gim, G. and Nikravesh, P.E. (1990) 'An analytical model of pneumatic tires for vehicle dynamic simulations. part 1: pure slips', *International Journal of Vehicle Design*, Vol. 11, No. 6, pp.589–618.

Li, B., Yang, X. and Yang, J. (2014) 'Tire model application and parameter identification-a. literature review', *SAE International Journal of Passenger Cars-Mechanical Systems*, Vol. 7, No. 2014-01-0872, pp.231–243.

Mavros, G. (2010) 'Chapter 23: contact mechanics of tyre-road interactions and its role in vehicle shuffle', in Rahnejat, H. (Ed.): *Tribology and Dynamics of Engine and Powertrain: Fundamentals, Applications and Future Trends*, Woodhead Publishing Limited, pp.703–734.

Oh, W. and Singh, R. (2005) *Examination of Clunk Phenomena using a Non-Linear Torsional Model of a Front Wheel Drive Vehicle with Manual Transmission*, SAE Technical Paper No. 2005-01-2291.

Pacejka, H. (2005) *Tire and Vehicle Dynamics*, Elsevier, Amsterdam.

Pacejka, H.B. and Bakker, E. (1992) 'The magic formula tyre model', *Vehicle System Dynamics*, Vol. 21, No. S1, pp.1–18.

Pawar, J., Biggs, S. and Jones, R.P. (2007) 'Sensitivity of system boundary conditions on the migration of low frequency modes controlling longitudinal vehicle response', *ASME 2007 International Design Engineering Technical Conferences and Computers and Information in Engineering Conference*, American Society of Mechanical Engineers, Las Vegas, USA, pp.517–524.

Sandu, C. and Umsrithong, A. (2014) 'Discrete mass tire model for ride investigation over uneven rigid terrain', *International Journal of Vehicle Design*, Vol. 66, No. 1, pp.87–106.

Svendenius, J. (2007) *Tire Modeling and Friction Estimation*, PhD thesis, Lund University, Lund, Sweden.

Wang, M.Y., Manoj, R. and Zhao, W. (2001) 'Gear rattle modelling and analysis for automotive manual transmissions', *Proceedings of the Institution of Mechanical Engineers, Part D: Journal of Automobile Engineering*, Vol. 215, No. 2, pp.241–258.

Wehrwein, D. and Mourelatos, Z.P. (2009) 'Optimization of engine torque management under uncertainty for vehicle driveline clunk using time-dependent metamodels', *Journal of Mechanical Design*, Vol. 131, No. 5, pp.051001.

Witzel, P. (2016) *Ein validiertes Reifenmodell zur Simulation des fahrdynamischen und fahrkomfortrelevanten Verhaltens von Ackerschleppern bei Hindernisüberfahrt*, PhD Thesis, University of Hohenheim, Stuttgart, Germany.

Wojewoda, J., Stefański, A., Wiercigroch, M. and Kapitaniak, T. (2008) 'Hysteretic effects of dry friction: modelling and experimental studies', *Philosophical Transactions of the Royal Society of London A: Mathematical, Physical and Engineering Sciences*, Vol. 366, No. 1866, pp.747–765.

Zegelaar, P.W.A. (1998) *The Dynamic Response of Tires to Brake Torque Variations and Road Unevennesses*, PhD thesis, Delft University of Technology, Delft, Netherlands.

Appendix

Table A1 Adopted values of parameters for the drivetrain model

Engine & Gearbox					
I_e ($\mathrm{kg \cdot m^2}$)	I_{g1} ($\mathrm{kg \cdot m^2}$)	$I_{g2}+I_{g3}$ ($\mathrm{kg \cdot m^2}$)	I_{g4} ($\mathrm{kg \cdot m^2}$)	K_c (Nm/rad)	C_c (Nms/rad)
0.5	0.0362/ 0.0372/ 0.1327	0.0429/ 0.0208/ 0.0015	0.0869	1500	3
Shafts & Axles					
I_{f0} ($\mathrm{kg \cdot m^2}$)	I_{f1} ($\mathrm{kg \cdot m^2}$)	I_{f2} ($\mathrm{kg \cdot m^2}$)	I_{f3} ($\mathrm{kg \cdot m^2}$)	I_{fa} ($\mathrm{kg \cdot m^2}$)	K_{f1} (Nm/rad)
0.02	0.015	0.03	0.01	8	35500
I_{r0} ($\mathrm{kg \cdot m^2}$)	I_{r1} ($\mathrm{kg \cdot m^2}$)	I_{r2} ($\mathrm{kg \cdot m^2}$)	I_{r3} ($\mathrm{kg \cdot m^2}$)	($\mathrm{kg \cdot m^2}$)	K_{f2} (Nm/rad)
0.02	0.015	0.03	0.01	8	19667
K_{r1} (Nm/rad)	K_{r2} (Nm/rad)	C_{f1} (Nms/rad)	C_{f2} (Nms/rad)	C_{r1} (Nms/rad)	C_{r2} (Nms/rad)
71000	19667	10	8	20	8
Tyre					
I_{fb} ($\mathrm{kg \cdot m^2}$)	M_{fb} (kg)	I_{rb} ($\mathrm{kg \cdot m^2}$)	M_{rb} (kg)	K_{ft} (Nm/rad)	K_{fb} (N/m)
109.52	200	109.52	200	5.40×10^5	3.51×10^6
K_{rt} (Nm/rad)	K_{rb} (N/m)	C_{ft} (Nms/rad)	C_{fb} (Ns/m)	C_{rt} (Nms/rad)	C_{rb} (Ns/m)
5.40×10^5	3.51×10^6	800	2000	800	2000
Vehicle					
M_v (kg)					
10200					

Table A2 Adopted gear ratios for the drivetrain model

Location	*Parameter*	*Ratio*
Gearbox (second gear ratio)	n_{g1}	1
	n_{g2}	2.84
Bevel gear pair	n_d	2.46
Planetary gear set	n_p	6